AFRL-AFOSR-VA-TR-2016-0328

Damage Precursor Detection in Polymer Matrix Composites Using Novel Smart Composite Particles

Aditi Chattopadhyay
ARIZONA STATE UNIVERSITY

09/20/2016
Final Report

Air Force Research Laboratory
AF Office Of Scientific Research (AFOSR)/ RTA1
Arlington, Virginia 22203
Air Force Materiel Command

DISTRIBUTION A: Distribution approved for public release.

REPORT DOCUMENTATION PAGE

Form Approved
OMB No. 0704-0188

1. REPORT DATE *(DD-MM-YYYY)*	2. REPORT TYPE	3. DATES COVERED *(From - To)*
28-09-2016	Final Performance	15 Jun 2012 to 14 Jun 2016

4. TITLE AND SUBTITLE
Damage Precursor Detection in Polymer Matrix Composites Using Novel Smart Composite Particles

5a. CONTRACT NUMBER

5b. GRANT NUMBER
FA9550-12-1-0331

5c. PROGRAM ELEMENT NUMBER
61102F

6. AUTHOR(S)
Aditi Chattopadhyay

5d. PROJECT NUMBER

5e. TASK NUMBER

5f. WORK UNIT NUMBER

7. PERFORMING ORGANIZATION NAME(S) AND ADDRESS(ES)
ARIZONA STATE UNIVERSITY
660 S MILL AVE STE 312
TEMPE, AZ 85281 US

8. PERFORMING ORGANIZATION REPORT NUMBER

9. SPONSORING/MONITORING AGENCY NAME(S) AND ADDRESS(ES)
AF Office of Scientific Research
875 N. Randolph St. Room 3112
Arlington, VA 22203

10. SPONSOR/MONITOR'S ACRONYM(S)
AFRL/AFOSR RTA1

11. SPONSOR/MONITOR'S REPORT NUMBER(S)
AFRL-AFOSR-VA-TR-2016-0328

12. DISTRIBUTION/AVAILABILITY STATEMENT
A DISTRIBUTION UNLIMITED: PB Public Release

13. SUPPLEMENTARY NOTES

14. ABSTRACT

A novel self-sensing framework, utilizing embedded cyclobutane-based mechanophores, was developed for identifying damage precursors and propagation. The novel 'smart' material was incorporated into a thermoset polymer matrix and the color change phenomenon was observed under compressive loading. The smart material based polymer system was used to construct glass fiver reinforced composites to investigate the performance of the composite under cyclic loading; the correlation between fluorescence intensity and fatigue cycle was investigated. Fourier Transform Infrared Spectroscopy showed the potential of detecting damage in carbon-containing composites by identifying changes in the peak intensity associated with the mechanically responsive cyclobutane ring. An atomistic simulation methodology was developed in conjunction with the experimental work; the Molecular Dynamics (MD) based methodology was capable of emulating the experiments. After simulating the epoxy curing and ultraviolet (UV) dimerization process, mechanophore activation in the thermoset polymer matrix was successfully emulated. A local work analysis method was developed to evaluate the mechanophore sensitivity quantitatively. The simulation method captured the physical entanglement between epoxy and mechanophore network, which affected the mechanical properties of the polymer matrix significantly. Results from the simulations showed increment in the number of activated cyclobutanes during the deformation test. Good agreement was observed with experimental results: the intensity of fluorescence was found to be directly proportional to the deformation.

15. SUBJECT TERMS
Polymer Matrix Composites

16. SECURITY CLASSIFICATION OF:			17. LIMITATION OF ABSTRACT	18. NUMBER OF PAGES	19a. NAME OF RESPONSIBLE PERSON
a. REPORT	b. ABSTRACT	c. THIS PAGE			FILLERUP, JAMES
Unclassified	Unclassified	Unclassified	UU		19b. TELEPHONE NUMBER *(Include area code)* 703-588-8316

Damage Precursor Detection in Polymer Matrix Composites Using Novel Smart Composite Particles

Final Performance Report
Reporting Period: June 2012 to September 2016

Program Manager: Dr. David Stargel

Grant No. FA95550-12-1-0331

Principal Investigator: Aditi Chattopadhyay

Co- Principal Investigator: Lenore L. Dai

Arizona State University

1. Project Objectives

Material Synthesis and Experiment:

- Synthesize cyclobutane-based mechanophores to impart stress-induced color changing capability to a thermoset polymer matrix to act as a damage sensor
- Develop cyclobutane-based smart polymers for incorporation into glass fiber-reinforced epoxy composite systems for fatigue damage detection and microcrack sensing via fluorescence emission
- Investigate the use of Fourier Transform Infrared (FTIR) Spectroscopy for a novel, alternative method for stress sensing, allowing for mechanophore application to previously not studied carbon-containing composites

Atomistic Scale Simulation:

- Develop a novel modeling framework to analyze mechanophore activation energy under complex mechanical loading conditions, which can reduce the number of necessary experiments and provide guidelines to design improved mechanophore embedded nanocomposites
- Simulate the epoxy curing process for the epoxy-based thermoset polymer matrix which accommodates the mechanophore (smart material) and transfers external force (stress) to the smart materials
- Emulate the ultra-violet (UV) dimerization for cyclobutane-based mechanophores (smart material) observed in experiments with epoxy curing simulation
- Implement a methodology for simulating mechanophore activation of a smart polymer matrix consisting of mechanophores, epoxy resin, and hardener
- Analyze force/energy distribution in the smart polymer system and investigate physical parameters responsible for mechanophore activation

2. Approach and Accomplishments

Task 1: Synthesis and Characterization of Smart Composite Particles

Thermoset polymers are generally quite brittle, with a propensity to crack if exposed to sufficient stress and strain, leading to irreversible damage such as microcracking. In order to detect micro damage, mechanophores, stress-induced color-changing materials, were synthesized and incorporated into an epoxy matrix. Two different types of cyclobutane-based mechanophores were used in this research: 1,1,1-tris(cinnamoyloxymethyl)ethane (TCE) and poly(vinyl cinnamate) (PVCi). The cyclobutane-based mechanophores were produced by photodimerization of the C=C double bonds from the cinnamoyl functional groups of TCE and PVCi. The cyclobutane structure has been proven to generate fluorescence emission upon the cleavage of the cyclobutane rings, indicating locations of microcracking in the mechanophore-embedded thermoset polymer (smart polymer). In this research, the effect of the two aforementioned cyclobutane-based mechanophores on the thermal and mechanical properties of smart polymers and the relationship between the stress and fluorescence emission were investigated.

Preparation of Cyclobutane-based Polymers

Materials: Unless otherwise stated, all the materials and reagents listed below were used as received. 1,1,1-tris(hydroxymethyl)ethane (99%), cinnamoyl chloride (98%), tetrahydrofuran (≥99.9%), 4-(dimethylamino)pyridine (≥99%), dichloromethane (≥99.8%), ethanol (≥99.5%) and poly(vinyl cinnamate) (PVCi, average Mn 45,000-55,000) were purchased from Sigma-Aldrich. Sodium chloride (≥99%) and water (HPLC) were purchased from Fisher Scientific. Epoxy resin (digycidylether of bisphenol F, DGEBF) and epoxy hardener (diethylenetriamine, DETA) were purchased from Epoxy System Inc.

Synthesis of 1,1,1- tris(cinnamoyloxymethyl)ethane: 1,1,1-tris(hydroxymethyl)ethane (1.2 g, 10 mmol) and 4-(dimethylamino)pyridine (4.4 g, 36 mmol) were dissolved in 100 mL of tetrahydrofuran (THF). Cinnamoyl chloride (6.0g, 36 mmol) was dissolved in 30 mL of THF. The two aforementioned solutions were then mixed together with a medium stirring speed and refluxed for 7 hours in a nitrogen atmosphere. The final mixture was dried with a rotary evaporator at reduced pressure in a water bath with the temperature controlled at 40-50 °C. After removing excess THF, beige colored solid powders were obtained. 30 mL of dichloromethane (CH_2Cl_2) was added to dissolve the impure solids. Next, the dissolved solution was washed three times with 15 mL of saturated aqueous sodium chloride. A crude product was obtained upon the evaporation of the solvent from the organic layer. The insoluble solids were removed via the application of hot ethanol. The prepared mixture was covered and left to cool over night at room temperature. Following cooling, a white crystalline product was precipitated from the prepared solution. The product was collected through filtration and washing with cold ethanol. Next, the final product was dried in a vacuum oven overnight at room temperature to obtain 3.5 g (68 % yield). The chemical structure of TCE was confirmed by NMR. ^{1}H NMR and ^{13}C NMR spectra were recorded on a Bruker 400 MHz spectrometer in a deuterated solvent, $CDCl_3$. All chemical shifts were reported in parts per million (ppm) with the internal tetramethylsilane (TMS) signal at 0.0 ppm as a standard. Mass spectra were recorded on a JEOL LCmate by scanning the magnet from m/z 200 to m/z 600. The ionization mode was atmospheric pressure chemical ionization (APCI), a chemical-ionization technique that uses gas-phase ion-molecule reactions at atmospheric pressure. The sample was prepared in dichloromethane/methanol (DCM/MeOH, 2:1, v/v).

Preparation of polymer blends (TCE and PVCi): To prepare a crosslinked TCE or PVCi polymer, a small amount of solid TCE or PVCi was first dissolved in CH_2Cl_2. The solution was poured into a clean silicon mold to form a thin film and was then placed in a vacuum to evaporate the excess CH_2Cl_2. All the silicon molds and glass slides used for sample preparation were pretreated with a mold release agent. After the excess CH_2Cl_2 evaporated, the thin film was photoirradiated at 302 nm for 4 hr. To prepare polymer/epoxy blends, the solution was added to DGEBF and dispersed well using an ultrasonic probe sonicator (Sonics VibraCell, 500 W model). The mixture was placed in a vacuum chamber at 50 °C to evaporate the CH_2Cl_2 until the mass of the mixture remained constant for an extended period of time, indicating that the excess CH_2Cl_2 had evaporated. The resin mixture was cooled down to room temperature before DETA was added and mixed ($M_{TCE\ or\ PVCi} : M_{Epoxy}$=1:10; $M_{DGEBF} : M_{DETA}$= 100:27). The mixture was sonicated in an ice bath to prevent any premature curing. After the mixture became homogenous, it was poured into the silicon molds and moved into a vacuum chamber to degas for 30 minutes, followed by photoirradiation conducted with a 302 nm wavelength UV lamp (UVP, UVM-28). According to the manufacturer's data, the light density is approximately 1300 $\mu W/cm^2$ at a distance of 3 cm. The sample was exposed to UV for 4 hours and cured overnight at room temperature. Preparation of the neat epoxy sample followed a similar procedure. After simple machining, the samples were ready for testing. The average dimensions of the samples were $3\times4\times8$ mm^3. For dynamic mechanical analysis (DMA), the mixture was poured onto a flat silicon surface with a glass cover placed on top. To make polymer/epoxy thin film, the uncured epoxy was compressed between two glass slides.

Preparation of glass fiber reinforced composite (GFRC): Epoxy polymer mixture containing uncured epoxy and 10 wt. % TCE was taken in a clean beaker and poured on the glass fiber mats. The composite sheet was cured under a load of 50 kg for 10 minutes and photoirradiation for 4 hours under UV light at a 302 nm wavelength. In order to further improve performance, the composite sheets were post-cured at 60 °C overnight in an oven and allowed to cool gradually. The sample size for characterization was $30\times80\times0.4$ mm^3.

Characterization

Photochemical properties of crosslinked polymers: A UV-Vis spectrometer was used to confirm the dimerization of cinnamate functional groups and further study the reaction kinetics. All UV spectroscopic analyses were performed on a UV-Vis spectrometer (Perkin Elmer Lambda 18) which was equipped with a UV light source by a deuterium lamp ($\lambda<$ 319.2 nm) and a visible light ($\lambda>$ 319.2 nm) source by a tungsten halogen lamp to provide usable wavelength from 185-900 nm. The machine was turned on 30 minutes prior to experimental measurements in order to warm up and stabilize the halogen and deuterium lamps. 0.05 mg of TCE was dissolved in 4 ml of CH_2Cl_2 and the 4 ml TCE solutions were transferred to a quartz cuvette of 1 cm path length. Neat CH_2Cl_2 solution was used as reference. The solution spectra of absorbance were measured ranging from 200 nm to 400 nm. The wavelength scan intervals are set up to 4 nm with scan speed of 120 nm/min. For the "baseline" scan, one empty cuvette was placed in a single holder labeled "reference" and another empty cuvette of the same type in another holder labeled with "sample". After the "baseline" scan, the empty "reference" cuvette was filled with the neat solvent and the "sample" cuvette was filled with the sample solution. The cuvettes were then put back onto the holder for measurement. After the first absorbance measurement of the sample (before UV photoirradiation), the vial was taken out and exposed to the UV lamp for 15 minutes. The vial was put back into the holder and another absorbance measurement was taken. The

spectra of the samples were recorded before and after each exposure at selected intervals of time. For the measurement of the PVCi solution, 0.09 mg of PVCi was dissolved in 4 ml of CH_2Cl_2 and transferred to a clean cuvette. All measurements were performed using the same parameters at room temperature.

The Fourier transform infrared spectroscopy (FTIR) was used to further confirm the functional groups of interest. All the spectra were analyzed on Bruker IFS 66V/S FTIR spectrometer with OPUS 4.0 software. A mid-IR KBr beamsplitter was used. The detector setting was set as "DLATGS" and scanner velocity as "7;20.0KHz". Infrared (IR) transmission spectroscopy was performed in a vacuum using an FTIR spectrophotometer in the spectra region from 600 to 4000 cm^{-1} at a resolution of 2 cm^{-1} with an average of 64 scans. A clean KBr disk was placed into a spectrometer disk holder in the chamber. The chamber was evacuated to get rid of water vapor and CO_2. A small amount of TCE was dissolved in CH_2Cl_2 to prepare a dilute solution. A small drop of the solution was placed onto the KBr disk. The solution was spread out on the KBr disk and left without any disturbance. The disk was placed back onto the holder and the chamber was evacuated again. CH_2Cl_2 was then evaporated off in a vacuum at room temperature to form a very thin film. A spectrum of the sample was run. After the measurement was taken, the sample chamber was vented. The KBr disk was then exposed to the UV lamp for half an hour, put back onto the holder, and the experiment was repeated. The spectra of the samples were recorded before and after exposure to UV photoirradiation at room temperature. All the parameters were held constant through the FTIR analysis.

Thermal and mechanical properties of polymer blends: The effect of the addition of the crosslinked polymer to the epoxy on glass transition temperature (Tg) was studied. The measurements of Tg were carried out with differential scanning calorimeter thermal analysis (DSC). The experiments were performed in a nitrogen atmosphere using TA Instruments Q20. Throughout the DSC work, temperature and heat flow calibrations were performed following standardized procedures. After a heating and cooling cycle up to 70 °C with a heating ramp rate of 10 °C /min to eliminate the thermal history, Tg was analyzed from the data of the second heating scan from -20 to 120 °C at 10 °C/min, with the TA Universal Analysis software. All samples were contained in Tzero pans with lids. An empty pan with a lid was used as reference. Reference and sample pans were placed onto the holders, each of which was equipped with its own heater and temperature sensor. The masses of the samples were in the range of 6–9 mg on average.

Thermogravimetric analysis (TGA) monitors the amount and rate of change in the mass of a sample as a function of temperature or time as a sample is heated at a programmed rate in a controlled atmosphere. The measurements are primarily used to determine the thermal stabilities of materials. In our experiment, TGA was carried out using a TA Instruments TGA Q500 machine. The sample masses were in the range of 15 to 20 mg and were placed in a tared platinum crucible. All the samples were heated from 30 to 600 °C at a heating rate of 10 °C/min in nitrogen. The weight loss was monitored and recorded as a function of temperature.

DMA was also used to measure the glass transition temperature, storage modulus, and loss modulus. Crosslink density of the neat epoxy, the epoxy blended with TCE polymer, and the epoxy blended with PVCi polymer can be calculated through DMA. Experiments were performed in a tension mode using a TA Instruments Q800. Multi-Frequency/Strain was used. Thin films of polymeric blend were mounted onto the tension clamp and the temperature was ramped from 25 to 120 °C at a heating rate of 5 °C/min. The frequency was 1Hz under amplitude

control. The strain amplitude was set at 25 μm. The size of each sample was 0.2 - 0.5 mm in thickness, 4 - 7 mm in width, and 8 – 13 mm in length.

To verify the stress response of cyclobutane-based polymers by fluorescence generation, the polymers were first coated with a clean polyethylene substrate. The fluorescent images on the coating surface were taken before and after the substrate was bent. In order to establish the relationship between the stress and fluorescent signal, compression tests were conducted. In the compression test, the compressive stress-strain behavior of these systems was obtained by an MTS servo hydraulic test system, as shown in Figure 1. All the tests were conducted at room temperature. The samples were applied by silicone oil to minimize the friction between the compression plate and the samples. Tests were run in displacement control in the longitudinal direction at loading rate of 1 mm/min.

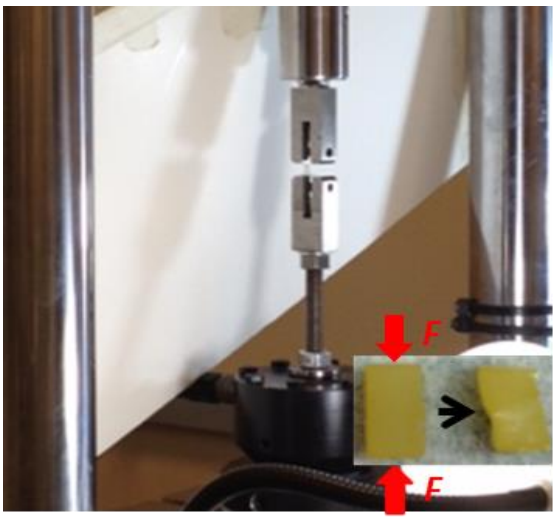

Figure 1. Cubic epoxy sample loaded on MTS servo hydraulic test system for compression test.

Fluorescence Response by Mechanically Activation

A small amount of TCE or PVCi was dissolved in CH_2Cl_2. The solution was applied to a polystyrene substrate to form a thin film, which was then placed into a vacuum oven in the dark to dry the solvent. The film was photoirradiated under a 302 nm wavelength UV lamp for 4 hours. The substrate was gently bent to generate cracks on the uncoated side of the substrate. The cracked surface was observed by an imaging system consisting of a phase contrast inverted microscope (Nikon Elipse TE300) outfitted with a Hamamatsu Orca 3CCD and a Olympus DP26 color camera that allows real-time digital image capture by exposure to 330-380 nm UV light. The emission filter was for wavelengths ranging between 435 – 485 nm.

To study the stress response of mechanophores, the neat epoxy and mechanophore embedded samples were punched with a hammer to generate cracks. Furthermore, the neat epoxy and mechanophore embedded samples were compressed to different strains. The compression was conducted on a MTS servo hydraulic test system. Tests were run in displacement control in the longitudinal direction at loading rate of 1 mm/min. The surface of the samples was monitored under the UV microscope. To calculate the fluorescent intensity on each image, the 8-bit fluorescent image was processed through ImageJ.

On the GFRC sheet, damage was applied with a metal tool. The fluorescence density changes were recorded and compared before and after damage through a fluorescent microscope. A uniaxial tensile fatigue test was performed on a GFRC sheet. First, a 4 mm wide notch in the center of the specimen was made to create an initial damage and to create a stress concentration on the area around the hole. Figure 2 shows the specimen loaded on the TestResource 800L test frame. The specimen was under the cyclic loading in a load-controlled mode at stress ratio (R), $\sigma_{min} / \sigma_{max}$=0.1 on a uniaxial fatigue frame operating with a sinusoidal waveform at a frequency of 2 Hz, as seen in Figure 3. Maximum stress (1000 N) and minimum stress (100 N) was constant for each cycle of a test. The number of fatigue cycles was recorded. After the application of a certain number of load cycles, the test was stopped. The specimen was dismounted and photographed under white light and a UV microscope. The specimen was then remounted and was once again subjected to cyclic loading. The fluorescence intensity at each fatigue cycle was calculated through ImageJ. The average data against cycles were plotted. The fatigue fracture surface of the specimen was sputter-coated with a thin layer of gold to observe the fatigue crack growth under scanning electron microscope (SEM). The specimens for SEM were sputter-coated with gold and viewed by SEM-XL30 (FEI). Specimens for SEM experiments were prepared by placing a piece of GFRC sheet onto newly cleaved mica substrate and applying Au coating of 10–15 nm thick using a sputter-coater.

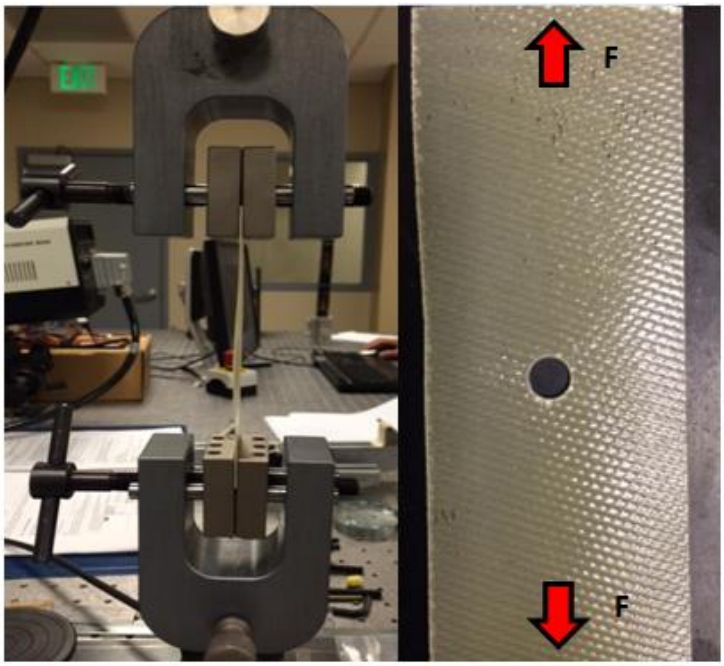

Figure 2**.** GFRC sheet loaded on the TestResource 800L test machine (left); GFRC sheet with a hole in the center before loaded (right).

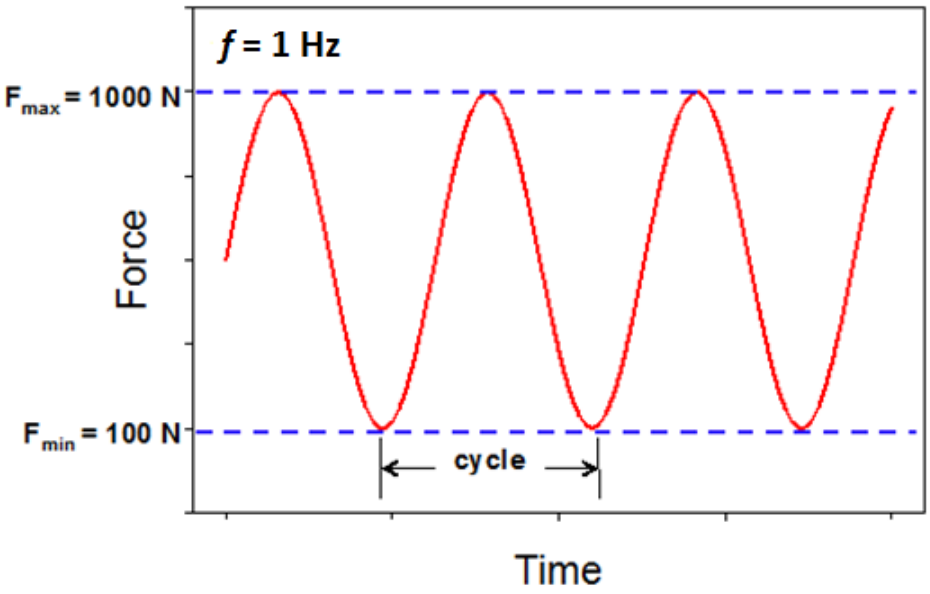

Figure 3. Cyclic loading parameter in tensile fatigue test.

Compression test: The goal for the application of cyclobutane-based polymer in its solid state was to demonstrate mechanochemical cleavage of covalent bonds, and to further investigate the use of these cyclobutane mechanophore blended with epoxy as stress/strain or damage sensors by visual detection. Epoxy material and composites with epoxy matrices are ubiquitous in everyday life, therefore it is very useful to detect the location of damage before an epoxy product undergoes failure. Here, a simple and direct method for detecting mechanochemical reactions with UV microscopy was applied because cyclobutane-based cross-linked polymers of tricinnamates have been reported to generate fluorescence upon the cleavage of cyclobutane rings. Cyclobutane, a four-membered ring molecule is known for its highly strained structure, largely attributed to angular and torsional strain. Therefore, the C-C bonds of cyclobutane is relatively weaker than other bonds such as C–O and other C–C bonds in the polymer structure. If cyclobutane is applied as a crosslinker in the crosslinked polymer, the mechanochemical cycloreversion of cyclobutane is the major reaction since it has lower bond strength.

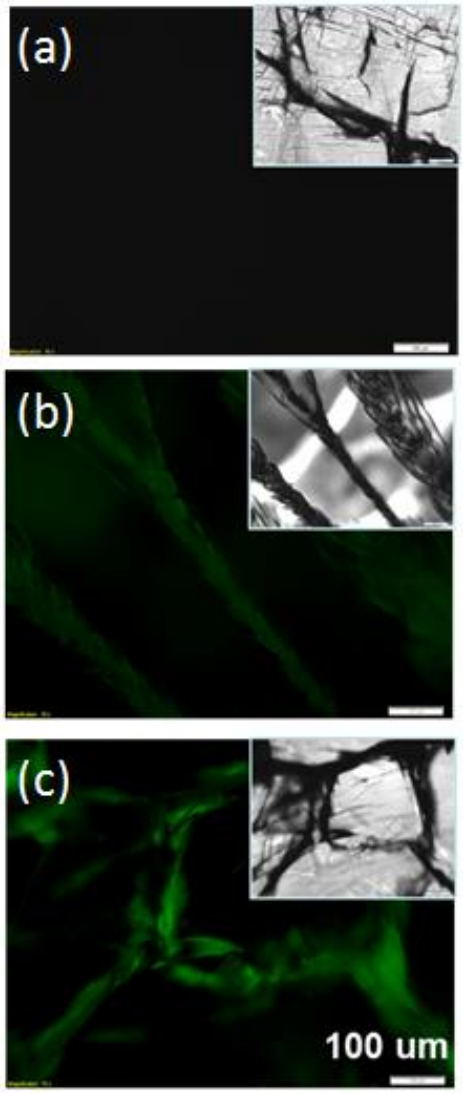

Figure 4. Microscopic images of cracks generated by hammer hit on (a) a clean polystyrene substrate, a polystyrene substrate coated with crosslinked (b)TCE and (c) PVCi polymer under a UV light. The insets were the corresponding images under a white light.

The fluorescence response was confirmed by coating crosslinked TCE polymer film on a polystyrene substrate at first. The cracks were generated by external force and observed using UV microscopy, as shown in Figure 4. Under the microscope with white light, the cracks were observed both on the polystyrene and polystyrene with coating. However, the fluorescent signal was only detected on the polystyrene coated with crosslinked TCE polymer exposed to UV light. Furthermore, crosslinked PVCi polymer was coated on the polystyrene substrate. The fluorescence emission was observed along the crack as well. The results indicated that the mechanochemical cleavage of cyclobutane occurred along the crack propagation and induced the fluorescence generation.

When the cracks were generated by an external force on the polymer blends with different amounts of crosslinked TCE polymer, fluorescence emission from the cracks was clearly observed under both UV and white light, as shown in Figure 5. The fluorescent signal was further augmented with increasing amount of crosslinked TCE polymer blended with epoxy. No fluorescence emission was found on neat epoxy under the same experimental conditions. From the images, epoxy with 10 wt. % crosslinked TCE polymer gave strong enough fluorescent emission to detect the damage. Thus, the content of 10 wt. % was used for the following fluorescent tests.

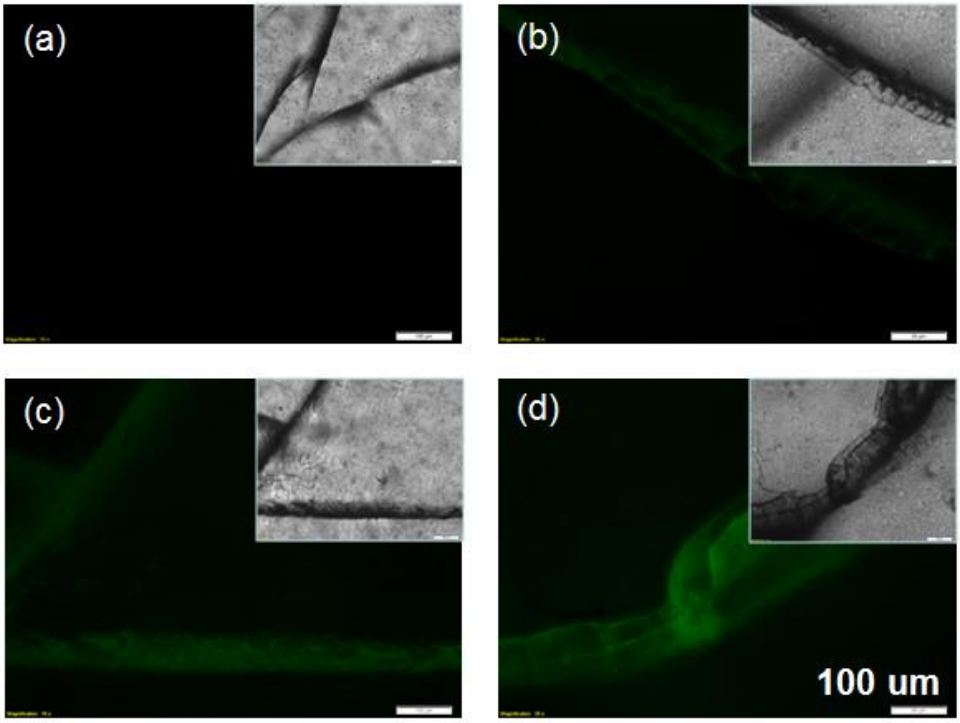

Figure 5. Microscopic images of fluorescence emission along cracks generated by hammer hit on polymer blends (a) without (b) with 10 wt.% (c) 30 wt. % (d) 50 wt.% crosslinked TCE polymer. The insets were the corresponding images under white light.

Neat epoxy and polymer blends were compressed to different strains. No fluorescence was detected on the neat epoxy. The evolution of induced fluorescence emission on epoxy is shown in Figure 6. For both polymer blends, there was not obvious fluorescence observed before the yield point was reached; right after the yield point, microcracks started to form and fluorescence emission could be observed under UV light. The cracks could not be clearly observed under white light, indicating that the fluorescence emission could provide a higher sensitivity and easier detection for the location of cracks, especially cracks at the microscale. It was also noticed that fluorescence emission along the crack intensified with strain after the yield point.

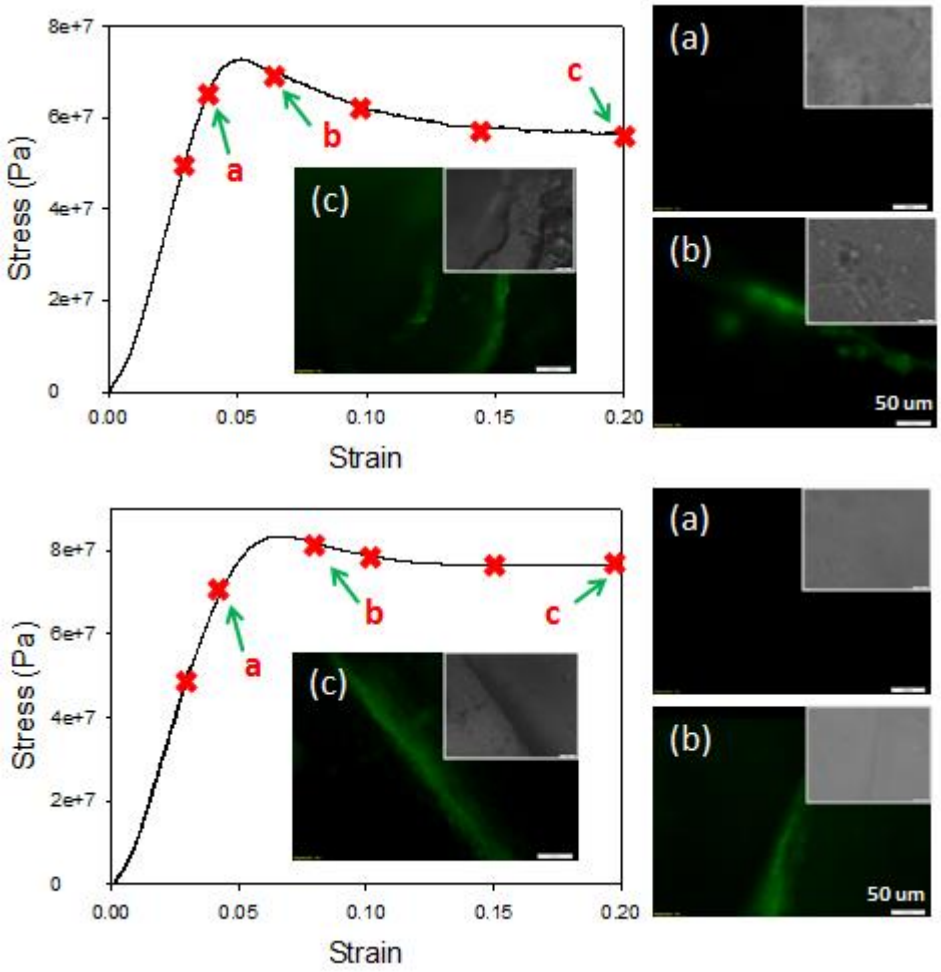

Figure 6. Microscopic images of fluorescence emission in response to different strains of epoxy w/ 10 wt. % crosslinked TCE (top) and PVCi (bottom) polymer blends.

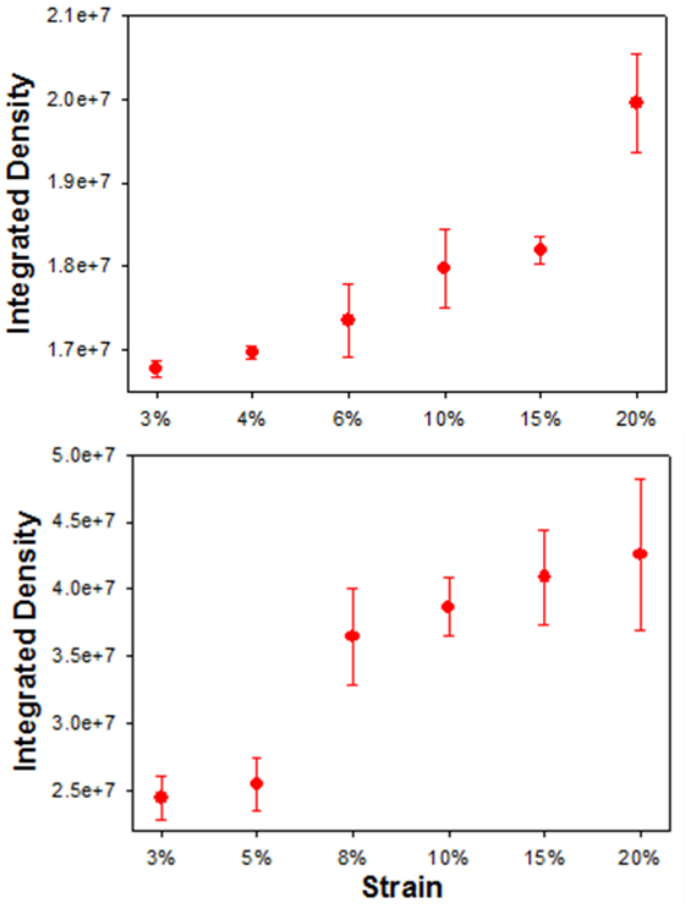

Figure 7. Integrated density of fluorescence emission in response to different strains of epoxy w/ 10 wt. % crosslinked TCE (top) and PVCi (bottom) polymer blends.

In order to further explore the relationship between the strains and their corresponding fluorescence response, ten fluorescent micrographs were processed by ImageJ and the average fluorescence densities were calculated. The density change as a function of strain was plotted and can be seen in Figure 7. As expected, the integrated densities increased with the accumulation of strain, which indicates that more cleavage of cyclobutane was activated with increasing strain.

Fatigue test: The fluorescence response on the GFRC was first confirmed by the damage applied with a metal tool. A circle was marked and the damage was made by the metal tool punch on one side of the single sheet within the circle, as seen in Figure 8 (right). The images within the circle, before and after the damage, were collected and compared. Obviously, the fluorescence was observed along the fiber after damage applied, as seen in Figure 8 (left).

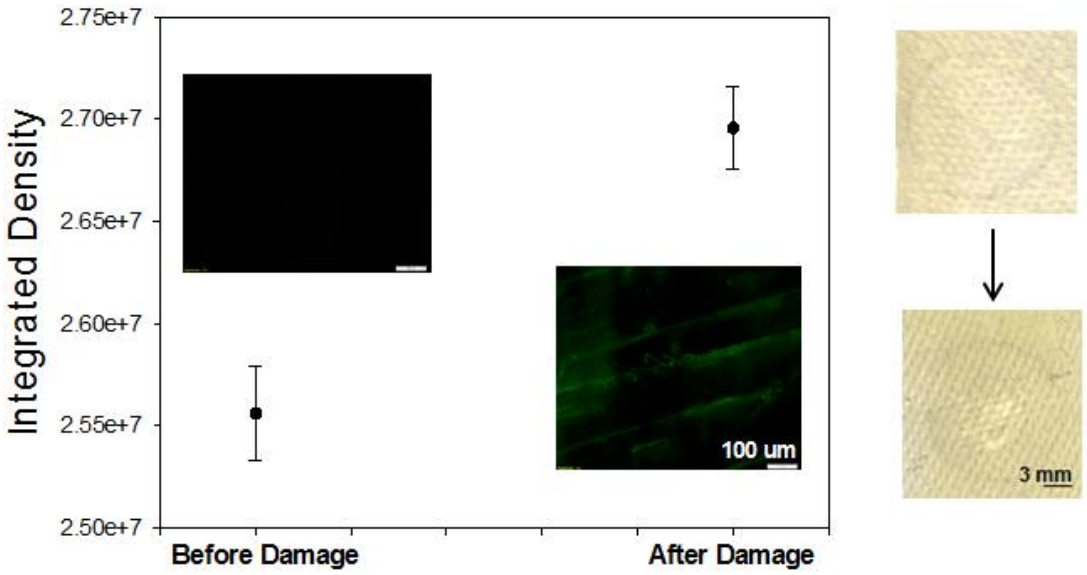

Figure 8. Fluorescence density of fiberglass epoxy composite with 10% TCE before and after damage was applied (left) and GFRC specimen under a white light (right).

The tensile fatigue failure is a common failure mode in most of the GFRC. A uniaxial tensile fatigue test was performed on a GFRC sheet. As mentioned before, the specimen was loaded cyclically in a load-controlled mode at stress ratio (R), σmin /σmax = 0.1 on a uniaxial fatigue frame operating with a sinusoidal waveform at a frequency of 2 Hz. Maximum stress (1000 N) and minimum stress (100 N) was constant for each cycle of a test. After a certain number of load cycles, the test was paused and the specimen was dismounted and photographed under white light and a UV microscope. The specimen was then remounted and the fatigue cycles were resumed. In order to monitor the crack growth on the GFRC specimen, SEM characterization of the specimen was carried out. Figure 9 shows the matrix cracks, matrix debonding, and fiber breakage on the GFRP specimen surface. Figure 9 (top) the shows microcracks on the matrix after 500 cycles. The exposure of glass fibers after 1,000 cycles in Figure 9 (middle) shows interface debonding. These exposed glass fibers tend to fracture under cyclic tensile force. After 1350 fatigue cycles, more breakage of glass fibers was observed as well as matrix cracks, causing a noticeable propagation along the longitudinal direction, as shown in Figure 9 (bottom). The corresponding macroscopic images are shown in Figure 9 (inset). With increasing fatigue cycles, the cracks developed in the 0°direction and became visible. The higher the number of fatigue cycles, the more cracks formed. UV microscopic images of fluorescence emission at different fatigue stages are shown in Figure 10. Damage initiated along the glass fibers in the 0° direction. With more cycles, the fluorescence emission became more obvious and the cracks along the glass fibers in the 90° direction grew as well. Fluorescent micrographs at different fatigue cycles were processed through ImageJ and the average fluorescence densities were calculated. The corresponding fluorescence density change was plotted in Figure 11. As expected, the density intensified as cycles increased, indicating that there were more cyclobutane molecules cleaved into cinnamate molecules due to the weaker bond strength on the cyclobutane ring than the other bonds.

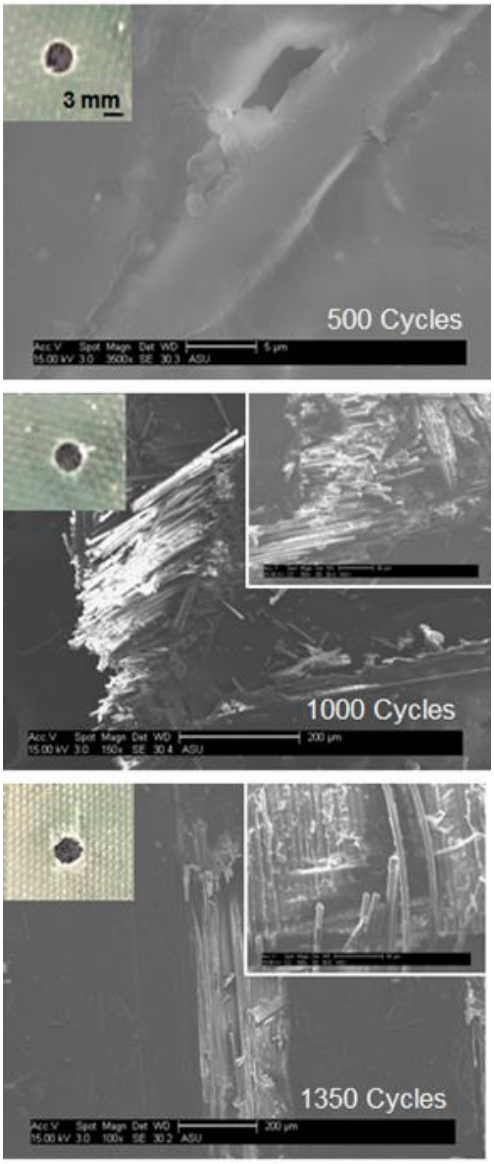

Figure 9. SEM micrographs of glass fiber reinforced epoxy composite with 10% TCE at different fatigue cycle stages. Insets are the images under white light.

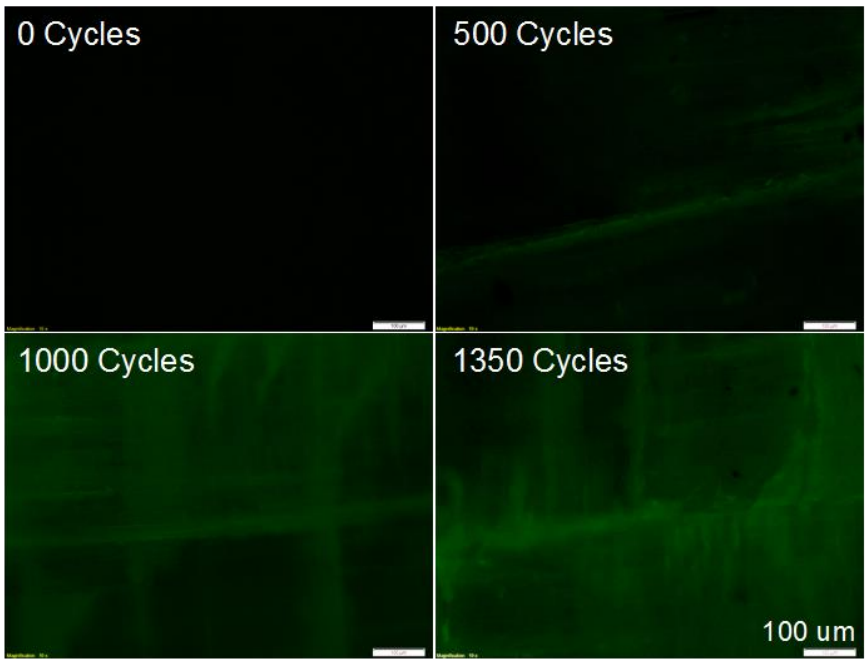

Figure 10. Microscopic images of fluorescence emission on GFRC in response to different fatigue cycle stages.

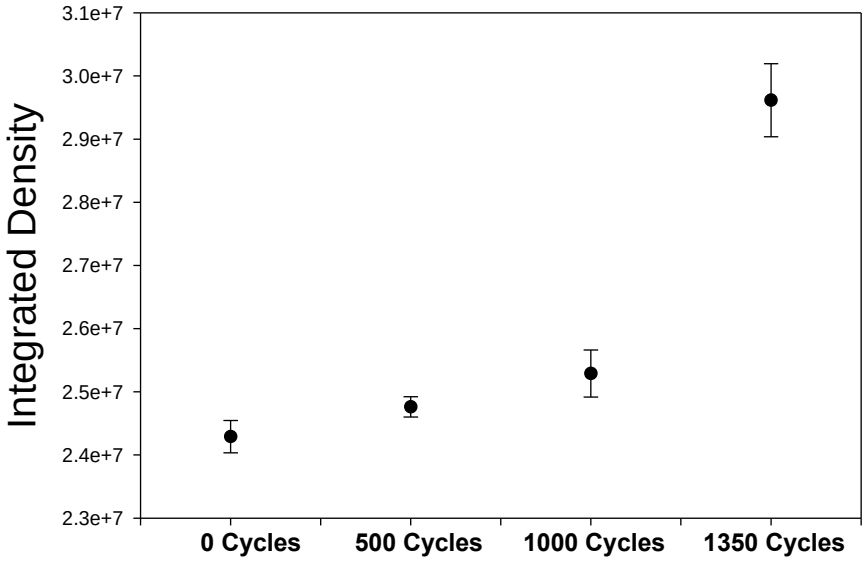

Figure 11. Corresponding fluorescence density of glass epoxy composite with 10% TCE at different fatigue cycle stages.

FTIR analysis: Results from FTIR were also used to track the functional groups during photoirradiation. Figure 12 shows the FTIR spectra of TCE film before and after irradiation with UV light. Before UV irradiation, two peaks were observed at 1713 cm^{-1} and 1637 cm^{-1}. These two peaks corresponded to the conjugated C=O stretching vibration and vinylene C=C stretching vibration, respectively. After 30 minutes of photoirradiation, the C=C peak disappeared. This can

be explained by the cyclobutane formation through photodimerization, which destroyed the conjugation in the entire π electron system. The C=O peak shifted to higher wavelength with decreasing absorbance, which can be attributed to the loss of π–conjugation from the C=C double bond. These observations were entirely consistent with the photo-crosslinking of cinnamoyl groups under UV photoirradiation and the spectral assignments, which are depicted schematically on the right hand side of Figure 12.

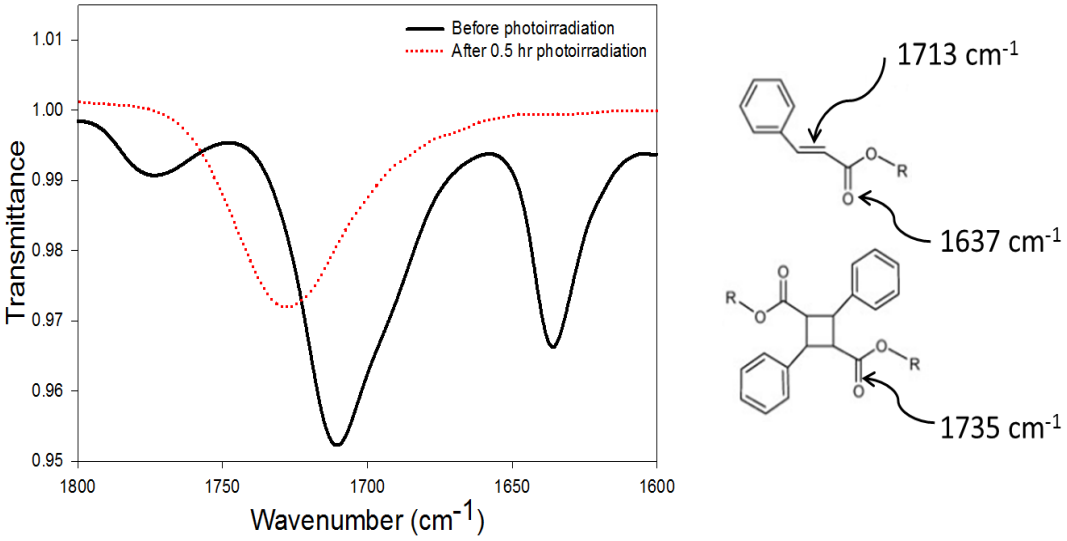

Figure 12. IR Spectra of TCE Film on a KBr Disk before and after Photoirradiation.

Task 2: Multiscale Modeling and Smart Composite Particle Fusion

A novel atomistic simulation framework capable of bridging the length scales from the quantum level to the macromolecular level was developed to simulate mechanophore activation in parallel with experiments. In experiments, TCE monomer was used to synthesize the cyclobutane structures through UV dimerization; the synthesized cyclobutanes were incorporated into a thermoset polymer matrix. A hybrid molecular dynamics (MD) simulation framework was developed by integrating two different force-fields: a classical force-field, Merck Molecular Force Field (MMFF), and a bond-order based force-field, Reactive Force Field (ReaxFF). This method facilitated the modeling of the epoxy-based thermoset matrix and simulation of the UV dimerization to construct cyclobutane-based mechanophores. The synthesis of the epoxy network and cyclobutane structure was numerically simulated by a covalent bond generation method by implementation of MMFF. Covalent bond dissociation leading to mechanophore activation was also simulated using ReaxFF. A local work analysis within the hybrid framework was developed to evaluate the sensitivity of mechanophores. Results from the simulation framework showed an increase in the number of activated cyclobutanes during the progression of the deformation test. Good agreement is observed with experimental results, for which the intensity of fluorescence was found to be directly proportional to the deformation.

Epoxy-based Thermoset Polymer Modeling

Constructing an accurate model capable of emulating the real epoxy-based thermoset polymer is very critical since mechanophore activation is determined by the structure surrounding the mechanophores. In order to simulate the curing process of the thermoset polymer, a cutoff distance based covalent bond generation method was developed. The accuracy of this curing simulation method was validated experimentally; the estimated Tgs of both neat epoxy and the smart polymer were compared with the experimental results obtained by DSC.

Unit cell preparation: Molecular structures of each component, epoxy resin (DGEBF) and hardener (DETA), were used to construct a neat epoxy unit cell in preparation for MD simulations. In order to construct the smart polymer unit cell, the molecular structure of TCE, which was used to make the mechanophore, was incorporated into the neat epoxy unit cell. A well-mixed epoxy-based system was guaranteed through a stochastic distribution of all the molecules. The number of molecules were determined by the weight ratio 100:27 (DGEBF:DETA) which was used for making experimental samples in this study. The weight of TCE was 10% of the total weight of the neat epoxy unit cell. Table 1 and Figure 13 show the calculated number of molecules and 3-D molecular structures in the smart polymer unit cell.

Table 1. Components of smart polymer (100:27 and 10% TCE).

	Weight	Formula	# of molecules
DGEBF	313 g/mol	$C_{19}H_{20}O_4$	65
DETA	103 g/mol	$C_4H_{13}N_3$	55
TCE	510 g/mol	$C_{32}H_{30}O_6$	5

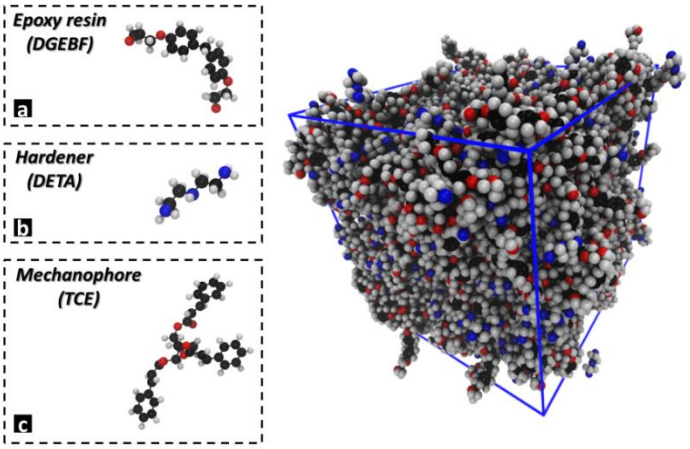

Figure 13. Schematic of smart polymer unit cell.

Simulation of epoxy curing process: In practice, epoxy resin and hardener generate covalent bonds stochastically when the distance between active sites of epoxy resin and hardener becomes less than a critical distance; in this space two active sites can share their electrons to make potential energy stable. This is known as the curing process in polymer science. Since the quality of the curing process affects the mechanical/thermal properties of epoxy-based thermoset system significantly, replicating this curing process via simulation is necessary to improve the reliability of the MD simulation results. Details of the curing process are as follows. First, the epoxide group of DGEBF and the amine group of DETA will maintain equilibrium distances by inter/intra molecular potential energy (stage 1 of Figure 14). Second, the carbon-oxygen bonds in the epoxide group and the nitrogen-hydrogen bonds in the amine group are broken. Third, from these separations, oxygen and hydrogen atoms react to generate O-H covalent bonds (stage 2 of Figure 14). Finally, the carbon of the epoxide group and nitrogen of the amine group react with each other and generate C-N covalent bonds (stage 3 in Figure 14). Figure 15 shows a 3-D visualization of DGEBF/DETA crosslinked systems. The red dotted lines in Figure 15(a) indicate that activated carbon atoms and activated nitrogen atoms react to generate C-N covalent bonds. DETA has three nitrogen atoms and can generate five C-N covalent bonds; both end nitrogen atoms have two active sties and the centered nitrogen atom has one active site (see Figure 17(c,d)). In addition to the C-N covalent bond generation, a photo-induced covalent bond generation for the cyclobutane structure should be considered. Figure 16 depicts the cyclobutane formation process, known as UV-induced [2 + 2] photocycloaddition, by which TCE monomers generate TCE polymers. After absorbing the UV-light energy, equilibrium of C=C double bonds (named cinnamoyl groups) is broken, leading to the generation of cyclobutane. In order to focus on the epoxy curing process in this section, the photo-induced crosslinking degree was fixed at 40%; numerical generation of cyclobutane will be covered in the next section. It must be noted that crosslinking degree was defined as the extent of cure: the ratio of the number of generated covalent bonds to the maximum number of possible bonds.

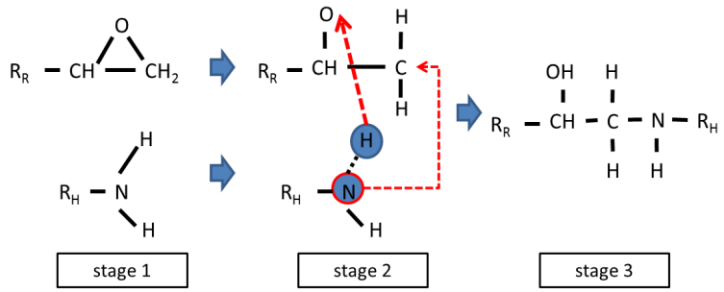

Figure 14. Procedure of covalent bond generation, where R_R is remaining part of resin, R_H is remaining part of hardener, C, N, H, and O are carbon, nitrogen, hydrogen, and Oxygen atom, respectively.

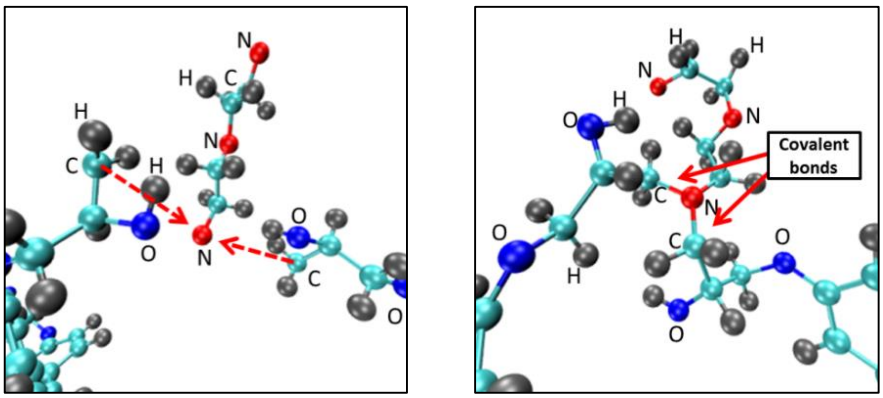

(a) Before bond generation (b) After bond generation

Figure 15. Schematic of molecular structure before and after covalent bond generation; grey, cyan, blue, and red spheres represent hydrogen, carbon, oxygen, and nitrogen, respectively.

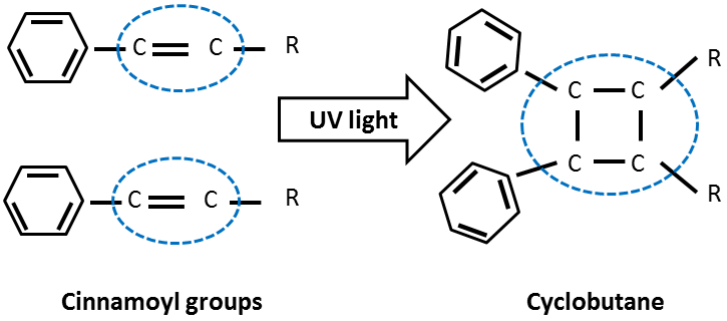

Figure 16. Schematic of procedure of cyclobutane generation using TCE monomers.

In order to emulate covalent bond generation between DGEBF and DETA in MD simulation, activated DGEBF and DETA molecules were prepared by removing five hydrogen atoms from three nitrogen atoms of DETA, and by changing the epoxide group to the methylene group as seen in Figure 17. With all the activated DGEBF and DETA molecules, and crosslinked TCE

molecules, the smart polymer unit cell for MD simulation was constructed. Periodic boundary conditions (PBC) were applied to the boundaries of the unit cell in all three directions (initial size of the unit cell is approximately 7 x 7 x 7 nm^3). After the initial configuration, conjugate gradient energy minimization was performed. Next, an NPT (isobaric-isothermal) ensemble simulation was conducted to equilibrate the unit cell using the Nose-Hoover thermostat and barostat to control temperature and pressure at 300K and 1atm for 150ps. The equilibration of the system was achieved when potential energy exhibited fluctuation around a constant mean value. Through the equilibration step, the molecules maintained minimum distances between active sties. Subsequently, the MD simulator generated covalent bonds when the distances between carbon and nitrogen atoms were within the cutoff distance of 4Å. Due to the stochastic nature of the phenomenon, there is no clearly validated cutoff distance for covalent bond generation in MD simulation available in the literature. The value of 4Å used in this study is equivalent to the van der Waals radii of a C-N bond; the closest distance that the active sites can approach one another before repulsion occurs. After generating C-N covalent bonds, hydrogen atoms were added to the activated nitrogen atoms, which failed to generate a covalent bond. With new covalent bonds being generated, the energy minimization process was performed to reduce undesired repulsive forces between atoms.

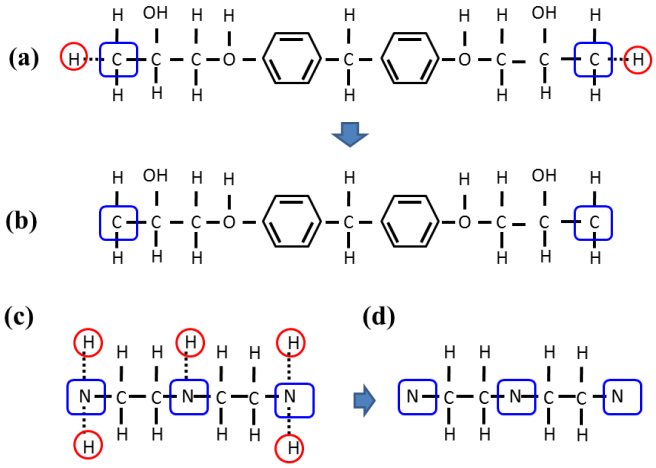

Figure 17. Chemical Structures of activated DGEBF and DETA: (a) pre-activated DGEBF; (b) activated DGEBF after removing two hydrogen atoms with red circle markings; (c) pre-activated DETA; (d) activated DETA after removing five hydrogen atoms with red circle markings.

Estimation of crosslinking degree: The development of an empirical model representing the crosslinking degree of the epoxy-based system was greatly complicated by the highly stochastic, material dependent nature of the crosslinking mechanism. Several numerical studies have been conducted to predict the crosslinking degree for different epoxy resins and hardeners. However, very few MD simulation results could be validated with experimental results. In this project, a purely stochastic approach to predict a most likely crosslinking degree for epoxy-based systems using MD simulation was utilized. Since this method was based on inter/intra molecular potential energy, it can be applied to any epoxy-based system. The methodology consisted of the following three steps: i) construct multiple unit cells with stochastic initial position of molecules, ii) generate numerical C-N covalent bonds for every unit cell, and iii) find average values of the crosslinking degree of all the unit cells. In this study 500 unit cells were constructed and C-N

covalent bonds were generated for all the unit cells using the numerical curing process. The number of unit cells was determined by an additional stochastic study using 1000 unit cells. As shown in Figure 18, the average crosslinking degree is measured as the number of unit cells increases. At the beginning of the plot, a fluctuation of the mean value was observed; however, the fluctuation diminished after using over 500 unit cells.

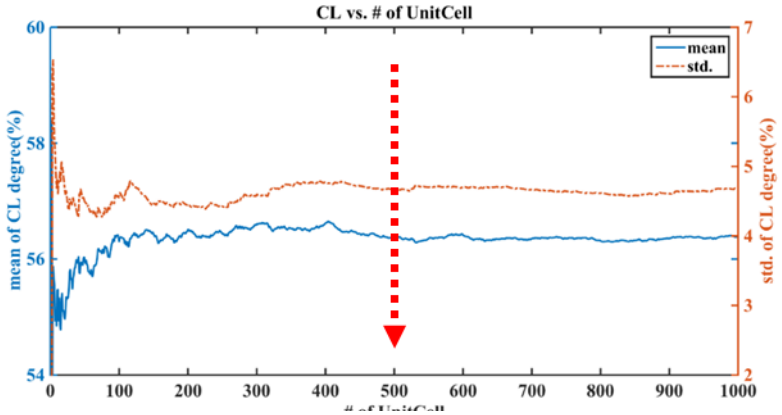

Figure 18. Average values of crosslinking (CL) degree vs. the number of unit cells.

Using the crosslinking degree data, a frequency distribution was plotted as seen in Figure 19. Calculated average crosslinking degrees are 56% and 52.7% for the neat epoxy and the smart polymer, respectively, which were considered the most likely crosslinking degrees in this project. Based on these values, representative neat epoxy and smart polymer unit cells were constructed to validate the MD simulation methodology. The values of Tg predicted by MD simulation, for both neat epoxy and smart polymer, were compared with the values measured by DSC. As seen in Figure 19, two asymptotic normal distributions were obtained from the histograms for both neat epoxy (mean value 56% and standard deviation 4.1%) and smart polymer (mean value 52.7% and standard deviation 4.2%).

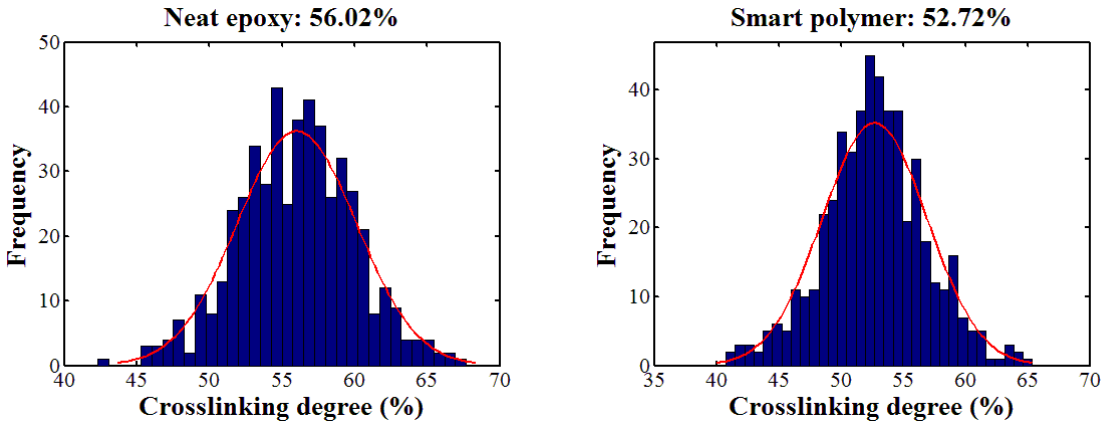

(a) (b)

Figure 19. Most likely crosslinking degrees of (a) neat epoxy and (b) smart polymer; red solid lines are fitted normal distributions.

Validation of epoxy curing simulation: Tgs were estimated by calculating densities at temperatures ranging from 250K to 450K using the systems with the most likely crosslinking

degrees (56% for neat epoxy and 52.7% for smart polymer). After generating covalent bonds, the system became unstable due to newly generated bonds. In order to ensure the stability of the system before initiating MD simulations with different temperatures, additional energy minimization and NPT ensembles (250K and 1atm for 200ps) were required. With a stabilized system, a stepwise heating simulation was performed by starting with an equilibrated system (250K and 1atm) and subsequently applying temperature increments of 10K. For each temperature, an NPT ensemble simulation has been conducted for 100ps. Compared to the experimental heating rate, 10K/100ps is very high; however, it is necessary because of the inherent time scale limitation of MD simulation. This discrepancy between the experimental and simulated heating rate was justified by making the assumption that once the system is equilibrated computationally, it will stay at the same state without any significant change, and the fact that 100ps was enough time to equilibrate the system. Densities at each temperature were calculated using the time average of densities around the equilibration state due to the fluctuating behavior of molecules. Figure 20 shows trends of density as a function of temperature for neat epoxy and smart polymer. Since the epoxy-based systems are amorphous polymers, there is a transition in density as the temperature varies. The temperature at the transition can be defined as Tg which was determined by locating the intersection of two linearly fitted lines in the two regions: glass and liquid state (Figure 20). Through this process, the Tgs of neat epoxy and smart polymer were predicted to be 345.2K and 320.8K, respectively. Table 2 shows the root mean squared error (RMSE) and R^2 to evaluate goodness-of-fit for the fitted linear curves. Since the RMSE and R^2 were close to 0 and 1, respectively, a linear fit to the MD simulation results was deemed appropriate for each region.

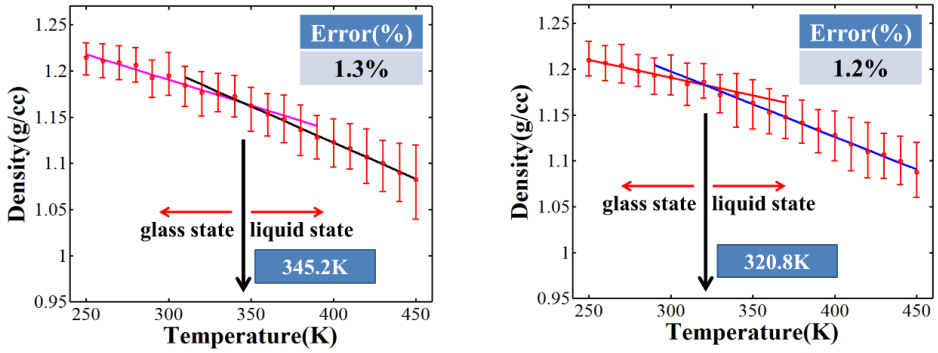

(a) Neat epoxy (b) Smart polymer

Figure 20. MD simulation results for Tg predictions.

Table 2. Evaluation of goodness-of-fit.

	Neat epoxy		Smart polymer	
	Glass state	Liquid state	Glass state	Liquid state
RMSE	0.0034	0.0015	0.002	0.0023
R^2	0.97	0.99	0.96	0.99

Estimated Tgs were also validated with experimental results. Experiments were conducted using DSC. A set of four experimental samples were fabricated for each material type: neat epoxy and smart polymer. The averaged values are presented in Figure 21. The comparisons between MD simulations and DSC results are shown in

Table 3 and show very good agreement between Tg values (within 2%). These results demonstrated the ability of the MD simulation framework to accurately describe the epoxy-based system, indicating a combination of force field MMFF and numerically simulating the crosslinking process is promising for epoxy-based studies. Furthermore, the results captured the influence of the smart material on the neat epoxy; a reduction in the Tg value. Based on these results, it is anticipated that the developed framework will be a reliable numerical method to evaluate thermal properties of other epoxy-based systems.

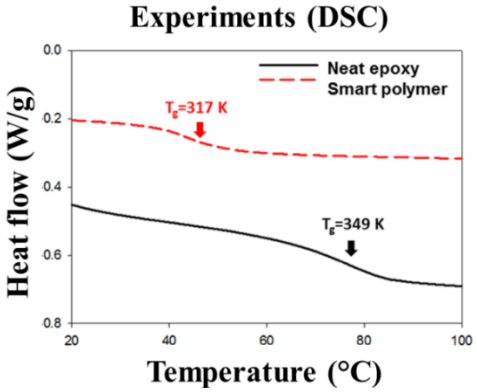

Figure 21. Tgs obtained by DSC: 349K for neat epoxy and 317K for Smart polymer.

Table 3. Percent error of each system.

	MD simulations	DSC	% Error
Neat epoxy	345.212K	349K	1.3%
Smart polymer	320.801K	317K	1.2%

UV Dimerization modeling

Quantum mechanics-based methods should be employed to capture the sub-molecular phenomena and quantify the energy difference induced by the deformed geometry of a single molecule. However, due to the high computational cost associated with quantum mechanics-based methods, a bond order-based force field MD simulation was used to investigate these sub-molecular phenomena in this work. A bond order-based force field MD simulation (different from the traditional MD simulation) can determine the potential energy of the molecular system as a function of a chemical bond such as a single bond, double bond, or triple bond. Since structural deformation initiates at the molecular level, it was clear that structural deformation causes mechanophore activation. The relationship between deformation energy and mechanophore activation energy needed to be addressed accurately. As a first step, mechanophore activation energy and local forces on mechanophores were investigated. All conditions, such as weight ratio and curing temperature/pressure, were determined via experiments.

Numerical dimerization: A cyclobutane-based mechanophore was synthesized in a thermoset polymer matrix using UV-induced [2+2] dimerization (also known as photocycloaddition) by which TCE monomers generate TCE polymers. The energy equilibrium of the cinnamoyl group (C=C) is broken after absorbing UV-light energy, which leads to the ring structure of four carbon

atoms known as cyclobutane. In order to implement numerical dimerization, a transformation of topology information was required. Figure 22 shows the difference in structure and bond length (which is directly related to topology) between TCE monomer and polymer. Considering there are huge differences in bond potential energies between single (348 kJ/mol) and double (614 kJ/mol) carbon bonds, it was important to assign correct topology information after generating cyclobutane structures. Especially since the C=C double bonds belonging to the cinnamoyl group affect neighbor atoms' topology, the neighbor atoms' topology should be changed accordingly when a double bond changes to a single bond. The numerical dimerization process included the following standard steps: i) Introduce more than two TCE monomers in a virtual unit cell (approximate size of the unit cell is 3 x 3 x 3 nm^3); ii) Equilibrate the unit cell using an NPT (isobaric-isothermal) ensemble at 300K and 1 atm with Nose-Hoover thermostat/barostat; iii) Generate covalent bonds when the carbon atoms belonging to the cinnamoyl group are within a certain distance of one another; iv) Assign correct topology information to the newly generated cyclobutane structure. Figure 23 shows that there are two possible types of cyclobutane structures. It was very critical to develop a method capable of implementing both types of cyclobutane structures to simultaneously achieve a high population of mechanophores and consecutive TCE monomer chain structures, which affects mechanical properties of the smart polymer as well as mechanophore activation because the TCE monomer chain is entangled with the epoxy polymer chain.

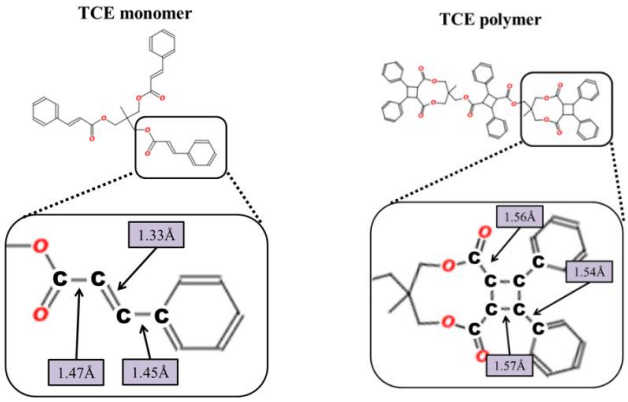

Bond	Length	Energy
C-C	1.54Å	348kJ/mol
C=C	1.34Å	614kJ/mol
C≡C	1.20Å	839kJ/mol

(a) (b)

Figure 22. (a) Topological difference between cinnamoyl group in TCE monomer and cyclobutane in TCE polymer (b) relationship between bond length and energy.

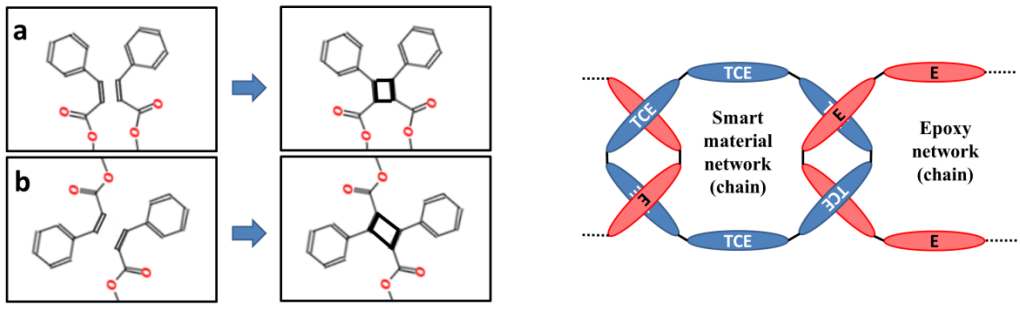

(a) (b)

Figure 23. (a) Two types of possible cyclobutane structures (b) schematic of physical entanglement between smart material network and epoxy network ('TCE': TCE monomers, 'E': epoxy molecule).

Verification of numerical dimerization: The numerical dimerization method was performed successfully; however, it was necessary to verify the reliability of the method. It is critical to check that the numerically dimerized TCE polymer has the correct topology information because irrelevant topology information would lead to incorrect dynamic behavior. Since new C-C covalent bonds were generated through the dimerization method, comparing bond dissociation energies (BDE) between pre-dimerized TCE polymer and numerically dimerized TCE polymer was the best way to check the reliability of the method. A bond order-based force field was used to implement constrained geometry external force (COGEF) in this work. Generally, COGEF is implemented in DFT-based software to calculate the BDE; however, BDE can be measured on a molecular dynamics simulator using the bond order-based force field. Unlike the empirical force field showing unrealistic increase in the covalent bond energy with an increase in bond length, the bond-order based force field shows that bond energy reaches a constant value above a bond length, indicating bond breakage. Also, note that the bond order-based force field is very useful for mechanophore activation analysis in the bulk polymer system (more than 100 TCE monomer system), because system size is not a critical issue unlike in quantum mechanics-based methods. One of the bond order-based force fields, reactive force field (ReaxFF), was used in this project. Compared to a quantum mechanics-based approach, which is required for quantifying the energy transition caused by covalent bond breakage/formation, ReaxFF can capture intramolecular interaction as well as interatomic interaction with high computational efficiency. COGEF includes the following standard steps: i) Energy minimization using conjugate gradient method; ii) NVT (isovolume-isothermal) ensemble equilibration for 10 ps until the potential energy of system reaches a certain value; iii) Tensile loading test by applying opposite direction forces to the covalent bonds belonging to cyclobutane-structure until dissociation. The trajectories of the atoms were saved every 100fs, and time averaged values of every state were saved every 1fs. The total energy of system was measured as the geometry changed, as shown in Figure 24. The tensile loading was stopped when the total energy dropped significantly, which indicated covalent bond dissociation. After bond breakage, an additional equilibration step was performed to find the potential energy state of damaged mechanophores. These simulation steps were applied to both TCE polymer systems: pre-dimerized cyclobutane and numerically dimerized cyclobutane. Figure 24 shows bond dissociation energies of 314.7kJ/mol and 315kJ/mol for pre-dimerized and numerically dimerized TCE polymer, respectively. The percentage error between the two systems was less than 0.001%, indicating the numerical dimerization method constructed the same cyclobutane structure as the pre-dimerized TCE polymer. These steps also revealed the amount of energy required for mechanophore activation. Additionally, the magnitude of the rupture force required to break the cyclobutane was investigated and determined to be 6.8 nN (nano-Newtons). This was very valuable information to analyze the force distribution inside the polymer system, especially for local atomic force transfer to carbon atoms in the cyclobutane as shown in Figure 25.

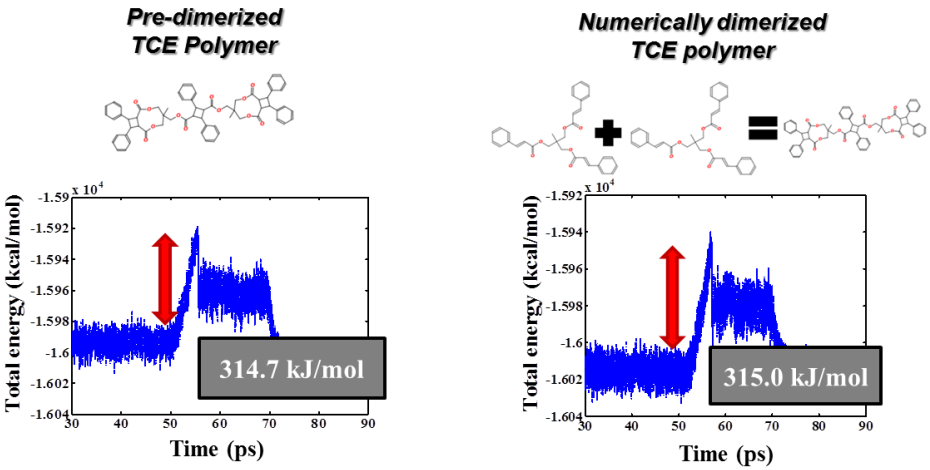

(a) (b)

Figure 24. Bond dissociation energy obtained from a) the pre-dimerized cyclobutane structure (TCE polymer), and b) numerically dimerized cyclobutane structure.

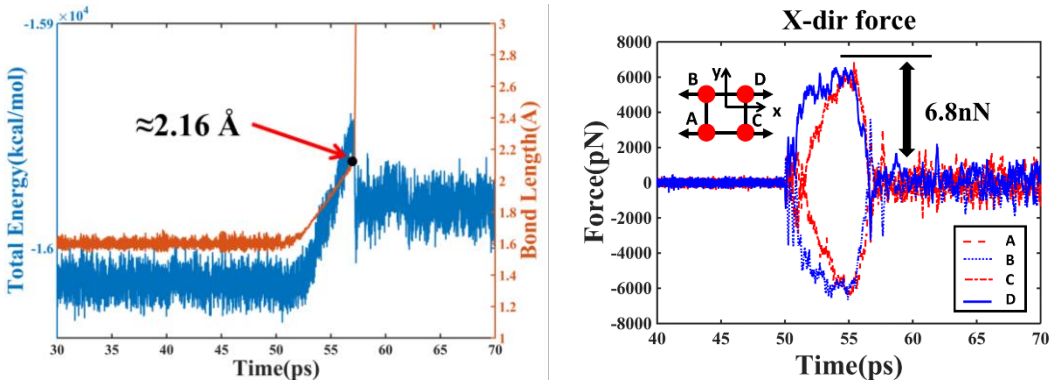

(a) (b)

Figure 25. a) C-C maximum bond lengths (2.16 Å), and b) BRF of cyclobutane (≈6.8 nN).

Virtual Loading Test and Local Force Analysis

Virtual loading test: A representative volume element (RVE) of the smart polymer consisted of randomly distributed molecules of the constituents. The weight percentages of the constituents, which were determined in experiments, were: 70 wt. % DGEBF, 20 wt. % DETA, and 10 wt. % TCE monomers. A 100-TCE monomer system was prepared and the number of resin/hardener molecules were determined accordingly as shown in Table 4 (84700 atoms). The use of a large number of TCE monomers was ideal since it would improve the likelihood of generating more cyclobutane structures; however, the analysis of a large system required a large amount of computational time. The 100-TCE monomer system generated an adequate number of cyclobutane structures in a reasonable simulation time, providing a good balance between fidelity and computational efficiency. Epoxy curing/UV dimerization simulations were first performed with MMFF and followed by virtual loading tests using ReaxFF. Periodic boundary conditions were applied to the boundaries of the RVE (approximate size: $50\times50\times50$ nm^3 at the initial state) along all three directions. Conjugate gradient energy minimization was performed.

Subsequently, NPT (isobaric-isothermal) ensemble equilibration was conducted on the RVE at 300K and 1atm (laboratory environment) for 10 ns using the Nose–Hoover thermostat and barostat to control the temperature and pressure, respectively. The 10 ns equilibration of the system allowed the potential energy to converge to a mean value with a small variance. After equilibration, the simulation of epoxy curing and UV dimerization were performed simultaneously; degrees of epoxy curing and UV dimerization reached to around 52% and around 28% (the number of new cyclobutane structures/the maximum possible number of cyclobutane structures), respectively. This was followed by system stabilization using an NPT ensemble again (300K and 1atm) to reduce the augmented potential energy caused by the newly generated bonds. After system stability was confirmed by checking the potential energy with a mean value and small variance, the virtual deformation tests were performed with ReaxFF. The quasi-static deformation method to capture plastic deformation of glassy polymers was employed for the virtual deformation tests of the crosslinked smart polymer unit cell. The atoms in the volume get remapped to new positions at each timestep while the simulation volume deforms. During the deformation, the cyclobutane ring-structures were stretched depending on the magnitude of applied force on the carbon atoms of cyclobutane. The atomic forces experienced by the mechanophore molecules were also stored for the local force/work analysis. It should be emphasized that the TCE polymer does not generate any covalent bonds with the epoxy network. As aforementioned, the physical entanglement between the epoxy network and TCE polymer chain allows load transfer, which leads to mechanophore activation.

Local work analysis: After the virtual deformation test, the mechanophore activation was analyzed using trajectory data of the atoms by monitoring the C-C bond lengths of cyclobutanes. The color change from red (healthy cyclobutane) to green (damaged cyclobutane) was triggered when the C-C bonds were stretched beyond the critical bond length (2.16 Å), as shown in Figure 26; however, this was based on a purely qualitative visualization approach. For quantitative simulation of the mechanophore activation, the atomic forces applied on the carbon atoms of cyclobutanes needed to be analyzed. The local force was defined as amplitude of an internal force which contributes to deformation of the C-C bonds. For example, if bond stretching forces, $\vec{F}_1$ and $\vec{F}_2$, were applied on the cyclobutane in opposite directions, as shown in Figure 27, the local force was specified by $\min\{|\vec{F}_1|,|\vec{F}_2|\}$ and the bond would move with an acceleration due to net force, $\vec{F}_{net}=\vec{F}_1+\vec{F}_2$. $\vec{F}_1$ and $\vec{F}_2$ were pair forces and canceled out if they were equal; however, the zero net force only implied zero acceleration of the bond, and the internal force ($|\vec{F}_1|=|\vec{F}_2|$) contributes to the deformation of the bonds. The local force definition is summarized in Table 3. Using this local force analysis approach, mechanophore activation was said to occur when one of the local forces of four bonds in the cyclobutane becomes greater than RBF (6.8nN). In order to verify whether the local force of cyclobutanes can trigger mechanophore activation, local force information of two different cyclobutanes in the RVE was monitored, whose activation states were already known from the previous visualization approach. The first cyclobutane chosen for this analysis had no activation and the second cyclobutane activated at 50% strain. Figure 28 shows the local force trends of the two cyclobutanes. However, the results indicate that local force analysis was not a relevant way to identify mechanophore activation, because the amplitudes of forces of the first cyclobutane (no activation) spike higher than the BRF (6.8nN) as the strain increases. In order to compensate for the local force analysis, a local work analysis approach was developed by considering the displacements of C-C bonds. The concept is equivalent to strain energy calculations used in structural analysis. The local work was defined as

the work ($\int \vec{F} \cdot d\vec{L}$) done by the applied local force ($\vec{F}$) on the bond with a small deformation $d\vec{L}$. This can be stated as $\int \min\{|\vec{F}_1|, |\vec{F}_2|\} \cdot d\vec{L}$ using the same example as shown in Figure 27. The results of local work analysis show that the dashed line AC (green) in Figure 29(b), in the case of the second cyclobutane, starts to increase at 50% strain. Essentially, a certain amount of force needs to be maintained over a certain amount of time to elongate a covalent bond until it breaks. Therefore, it was reasonable to claim that the local work is a key factor governing mechanophore activation, instead of local forces. Five samples with different initial locations of molecules and the same weigh fraction of constituents are generated and tested as a statistical study. The results show that the mechanophores in all the samples are consistently activated at a strain of approximately 25% and the number of activated mechanophores increases as the strain increases (see Figure 30).

Table 4. Components in the smart polymer (DGEBF:DETA:TCE=70%:20%:10%)

	Weight	Formula	Number of Molecules
DGEBF	313 g/mol	$C_{19}H_{20}O_4$	1300
DETA	103 g/mol	$C_4H_{13}N_3$	1100
TCE	510 g/mol	$C_{32}H_{30}O_6$	100

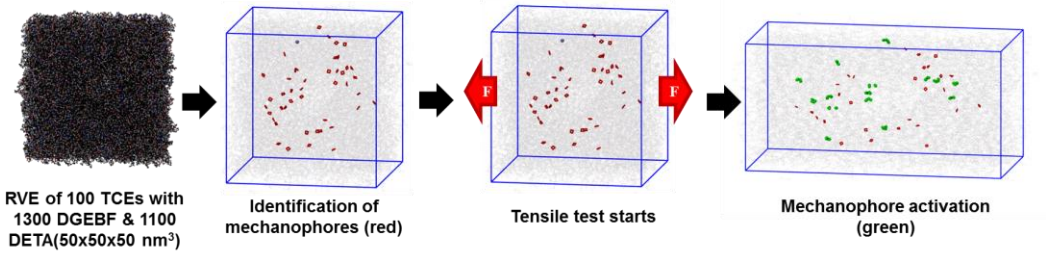

(a) (b) (c)

Figure 26. Procedure for simulation of mechanophore activation: a) prepare dimerized smart polymer RVE, b) start the deformation test (atoms in red represents healthy cyclobutanes, atoms in green represents damaged cyclobutanes), and c) observe atoms in green as the RVE deforms.

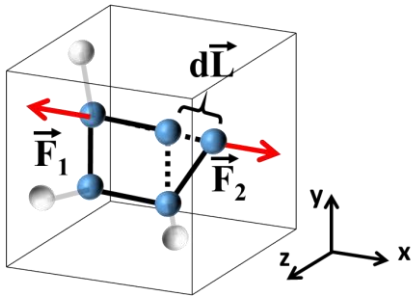

Figure 27. Schematic of cyclobutane under the applied atomic forces ($\vec{F}_1$ and $\vec{F}_2$); $d\vec{L}$ is displacement.

Table 5. Definition of local force due to $\vec{F}_1, \vec{F}_2$ along x-axis in opposite direction (Figure 27).

Condition of Atomic Force ($\vec{F}_1, \vec{F}_2$)	Local Force	Motion
$\lvert\vec{F}_1\rvert = \lvert\vec{F}_2\rvert$	$\min\{\lvert\vec{F}_1\rvert, \lvert\vec{F}_2\rvert\}$	zero acceleration
$\lvert\vec{F}_1\rvert \neq \lvert\vec{F}_2\rvert$		acceleration due to $\vec{F}_1 + \vec{F}_2$

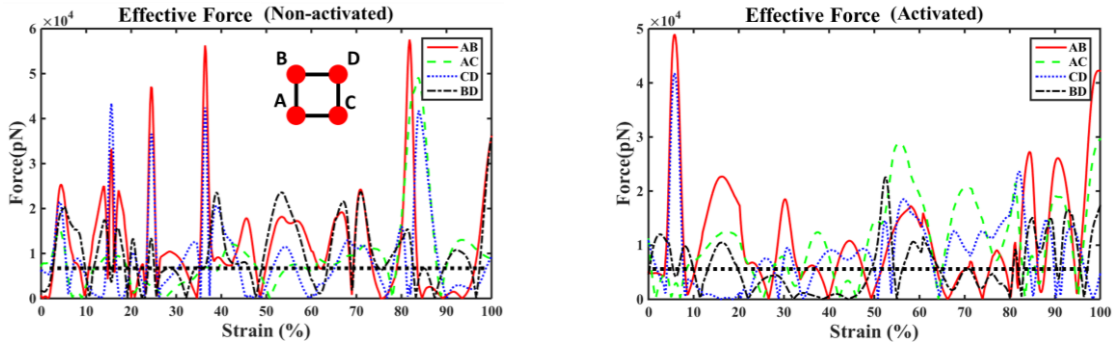

(a) (b)

Figure 28. Local force plots of two cyclobutanes in the polymer matrix: a) cyclobutane with no activation and b) activated cyclobutane at 50% strain (dotted black line represents the threshold of 6.8nN).

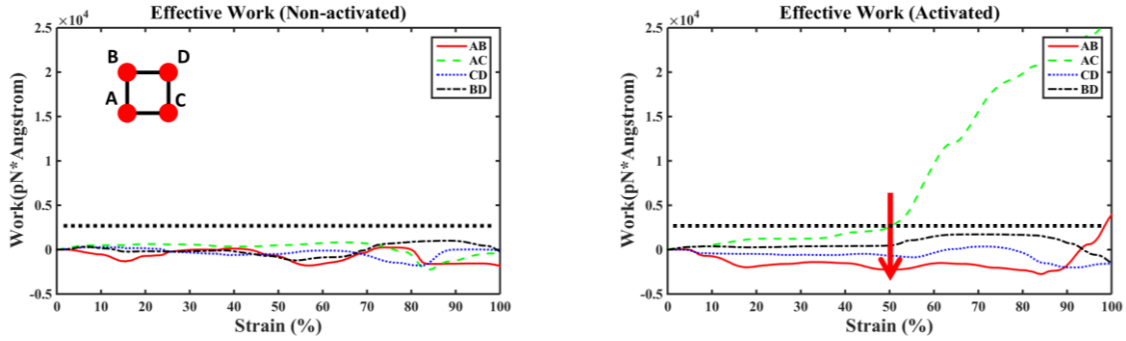

(a) (b)

Figure 29. Local work plots of two cyclobutanes in the polymer matrix: a) cyclobutane with no activation and b) activated cyclobutane at 50% strain (dotted black line represents the threshold of 315kJ/mol (=2,615 pN-Å)).

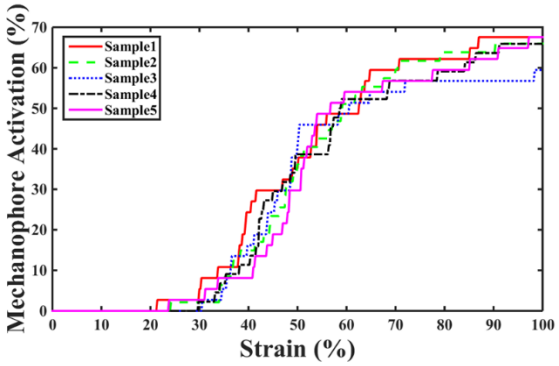

Figure 30. Mechanophore activation vs. strain.

3. Personnel Supported

Aditi Chattopadhyay	PI, Regents' Professor & Ira A. Fulton Chair Professor
Lenore L. Dai	Co-PI, Professor and Director
Yingtao Liu	Postdoctoral Fellow (Asst. Prof. at Univ. of Oklahoma)
Bonsung Koo	Graduate Research Associate (Mechanical Engineering)
Jin Zou	Ph.D. (Chemical Engineering, 2014)
Jinjun Zhang	Ph.D. (Mechanical Engineering, 2014)

4. Publications

Archival Journal Papers

1. Koo, B., Liu, Y., Zou, J., Chattopadhyay, A., & Dai, L. L., Study of glass transition temperature (Tg) of novel stress-sensitive composites using molecular dynamic simulation. *Modelling and Simulation in Materials Science and Engineering*, 22(6), (2014): 065018.
2. Zou, J., Liu, Y., Shan, B., Chattopadhyay, A., & Dai, L. L., Early damage detection in epoxy matrix using cyclobutane-based polymers. *Smart Materials and Structures*, 23(9), (2014): 095038.
3. Zhang, J., Koo, B., Subramanian, N., Liu Y., and Chattopadhyay, A., "An Optimized Cross-Linked Network Model to Simulate Smart Polymeric Material Response", *Journal of Intelligent Material Systems and Structures*, 24(8), (2015): 085022.
4. Zhang, J., Koo, B., Liu, Y.; Zou, J., Dai, L., and Chattopadhyay, A., "A Novel Statistical Spring-Bead Based Network Model for Self-Sensing Smart Polymer Materials", *Smart Materials and Structures*, (2015), DOI: 10.1177/1045389X15595292.
5. Zou, J., Liu, Y., Chattopadhyay, A., and Dai, L., "A self-sensing fiber reinforced polymer composite using mechanophore-based smart polymer", *Journal of Multifunctional Composites*, (2015).
6. Koo, B., Chattopadhyay, A., and Dai, L., Atomistic modeling framework for a cyclobutane-based mechanophore-embedded nanocomposite for damage precursor detection. *Computational Materials Science*, 120, 135-141 (2016).

Conference Papers

1. Zhang, J., Koo, B., Subramanian, N., Liu, Y., & Chattopadhyay, A. "Statistical Multiscale Modeling of Smart Polymer Materials using a Spring-Bead Based Network Model." Proc. of the AIAA SciTech Conference (2014)
2. Koo, B., Liu, Y., Chattopadhyay, A., and Dai, L. "Multiscale Modeling of a Mechanophore-embedded Nanocomposite for Damage Initiation Detection", *Proc.* AIAA SciTech 2015.
3. Koo, B., Nofen, E., Chattopadhyay, A., and Dai, L., "Multiscale Modeling and Characterization of Stress-Sensitive Mechanophore-Embedded Nanocomposite", *Proc.* IWSHM September 2015.
4. Johnston, J., Koo, B., Subramanian, N., and Chattopadhyay, A., "Implementation of a Molecular Interphase Model within a Multiscale Framework for Polymer Matrix Composites", *Proc.* ICCM July 2015.
5. Nofen, E., Zou, J., Wickham, J., Chattopadhyay, A., and Dai, L., "Damage Precursor Detection in Polymer Matrix Composites", *Proc.* American Chemical Society National Meeting, March 2015.
6. Zhang, J., Koo, B., Liu, Y., and Chattopadhyay, A., "Statistical Multiscale Modeling of Bond Clusters in Smart Polymer using Coupled Molecular Dynamics and Spring-Damper Model", *Proc.* AIAA SciTech, 2014.
7. Zou, J., Liu, Y., Chattopadhyay, A., & Dai, L. (2015, April). A self-sensing fiber reinforced polymer composite using mechanophore-based smart polymer. In SPIE Smart Structures and Materials and Nondestructive Evaluation and Health Monitoring (pp. 943204-943204). International Society for Optics and Photonics.

AFOSR Deliverables Submission Survey

Response ID:6880 Data

1.

Report Type

Final Report

Primary Contact Email

Contact email if there is a problem with the report.

aditi@asu.edu

Primary Contact Phone Number

Contact phone number if there is a problem with the report

480-965-9342

Organization / Institution name

Arizona State University

Grant/Contract Title

The full title of the funded effort.

Damage Precursor Detection in Polymer Matrix Composites Using Novel Smart Composite Particles

Grant/Contract Number

AFOSR assigned control number. It must begin with "FA9550" or "F49620" or "FA2386".

FA9550-12-1-0331

Principal Investigator Name

The full name of the principal investigator on the grant or contract.

Aditi Chattopadhyay

Program Officer

The AFOSR Program Officer currently assigned to the award

Mr. James Fillerup

Reporting Period Start Date

06/14/2012

Reporting Period End Date

09/14/2016

Abstract

A novel self-sensing framework, utilizing embedded cyclobutane-based mechanophores, was developed for identifying damage precursors and propagation. The novel "smart" material was incorporated into a thermoset polymer matrix and the color change phenomenon was observed under compressive loading. The smart material based polymer system was used to construct glass fiver reinforced composites to investigate the performance of the composite under cyclic loading; the correlation between fluorescence intensity and fatigue cycle was investigated. Fourier Transform Infrared Spectroscopy showed the potential of detecting damage in carbon-containing composites by identifying changes in the peak intensity associated with the mechanically responsive cyclobutane ring. An atomistic simulation methodology was developed in conjunction with the experimental work; the Molecular Dynamics (MD) based methodology was capable of emulating the experiments. After simulating the epoxy curing and ultraviolet (UV) dimerization process, mechanophore activation in the thermoset polymer matrix was successfully emulated. A local work analysis method was developed to evaluate the mechanophore sensitivity quantitatively. The simulation method captured the physical entanglement between epoxy and mechanophore network, which affected the mechanical properties of the polymer matrix significantly.

Results from the simulations showed increment in the number of activated cyclobutanes during the deformation test. Good agreement was observed with experimental results: the intensity of fluorescence was found to be directly proportional to the deformation.

Distribution Statement

This is block 12 on the SF298 form.

Distribution A - Approved for Public Release

Explanation for Distribution Statement

If this is not approved for public release, please provide a short explanation. E.g., contains proprietary information.

SF298 Form

Please attach your SF298 form. A blank SF298 can be found here. Please do not password protect or secure the PDF The maximum file size for an SF298 is 50MB.

sf298_AditiChattopadhyay.pdf

Upload the Report Document. File must be a PDF. Please do not password protect or secure the PDF . The maximum file size for the Report Document is 50MB.

AFOSR Final Report 2016_Aditi_Chattopadhyay.pdf

Upload a Report Document, if any. The maximum file size for the Report Document is 50MB.

Archival Publications (published) during reporting period:

Archival Journal Papers

1. Koo, B., Liu, Y., Zou, J., Chattopadhyay, A., & Dai, L. L., Study of glass transition temperature (Tg) of novel stress-sensitive composites using molecular dynamic simulation. Modelling and Simulation in Materials Science and Engineering, 22(6), (2014): 065018.
2. Zou, J., Liu, Y., Shan, B., Chattopadhyay, A., & Dai, L. L., Early damage detection in epoxy matrix using cyclobutane-based polymers. Smart Materials and Structures, 23(9), (2014): 095038.
3. Zhang, J., Koo, B., Subramanian, N., Liu Y., and Chattopadhyay, A., "An Optimized Cross-Linked Network Model to Simulate Smart Polymeric Material Response", Journal of Intelligent Material Systems and Structures, 24(8), (2015): 085022.
4. Zhang, J., Koo, B., Liu, Y.; Zou, J., Dai, L., and Chattopadhyay, A., "A Novel Statistical Spring-Bead Based Network Model for Self-Sensing Smart Polymer Materials", Smart Materials and Structures, (2015), DOI: 10.1177/1045389X15595292.
5. Zou, J., Liu, Y., Chattopadhyay, A., and Dai, L., "A self-sensing fiber reinforced polymer composite using mechanophore-based smart polymer", Journal of Multifunctional Composites, (2015).
6. Koo, B., Chattopadhyay, A., and Dai, L., Atomistic modeling framework for a cyclobutane-based mechanophore-embedded nanocomposite for damage precursor detection. Computational Materials Science, 120, 135-141 (2016).

Conference Papers

1. Zhang, J., Koo, B., Subramanian, N., Liu, Y., & Chattopadhyay, A. "Statistical Multiscale Modeling of Smart Polymer Materials using a Spring-Bead Based Network Model." Proc. of the AIAA SciTech Conference (2014)
2. Koo, B., Liu, Y., Chattopadhyay, A., and Dai, L. "Multiscale Modeling of a Mechanophore-embedded Nanocomposite for Damage Initiation Detection", Proc. AIAA SciTech 2015.
3. Koo, B., Nofen, E., Chattopadhyay, A., and Dai, L., "Multiscale Modeling and Characterization of Stress-Sensitive Mechanophore-Embedded Nanocomposite", Proc. IWSHM September 2015.
4. Johnston, J., Koo, B., Subramanian, N., and Chattopadhyay, A., "Implementation of a Molecular Interphase Model within a Multiscale Framework for Polymer Matrix Composites", Proc. ICCM July 2015.
5. Nofen, E., Zou, J., Wickham, J., Chattopadhyay, A., and Dai, L., "Damage Precursor Detection in Polymer Matrix Composites", Proc. American Chemical Society National Meeting, March 2015.
6. Zhang, J., Koo, B., Liu, Y., and Chattopadhyay, A., "Statistical Multiscale Modeling of Bond Clusters in Smart Polymer using Coupled Molecular Dynamics and Spring-Damper Model", Proc. AIAA SciTech, 2014.
7. Zou, J., Liu, Y., Chattopadhyay, A., & Dai, L. (2015, April). A self-sensing fiber reinforced polymer

composite using mechanophore-based smart polymer. In SPIE Smart Structures and Materials and Nondestructive Evaluation and Health Monitoring (pp. 943204-943204). International Society for Optics and Photonics.

New discoveries, inventions, or patent disclosures:

Do you have any discoveries, inventions, or patent disclosures to report for this period?

No

Please describe and include any notable dates

Do you plan to pursue a claim for personal or organizational intellectual property?

Changes in research objectives (if any):

Change in AFOSR Program Officer, if any:

Dr. David Stargel (previous)
Mr. James Fillerup (current)

Extensions granted or milestones slipped, if any:

AFOSR LRIR Number

LRIR Title

Reporting Period

Laboratory Task Manager

Program Officer

Research Objectives

Technical Summary

Funding Summary by Cost Category (by FY, $K)

	Starting FY	FY+1	FY+2
Salary			
Equipment/Facilities			
Supplies			
Total			

Report Document

Report Document - Text Analysis

Report Document - Text Analysis

Appendix Documents

2. Thank You

E-mail user

Sep 14, 2016 16:07:14 Success: Email Sent to: aditi@asu.edu